Reduced Complexity Models for Water Management and Anode Purge Scheduling in DEA Operation of PEMFCs

Jason B. Siegel[a], Serhat Yesilyurt[b], and Anna G. Stefanopoulou[c]

[a] Engineering, University of Michigan, Ann Arbor MI, 48109, USA
[b] Sabanci University, Orhanli-Tuzla, 34956 Istanbul, Turkey
[b] Mechanical Engineering, University of Michigan, Ann Arbor MI, 48109, USA

In this work, the dynamic behavior of Fuel Cell operation under Dead-Ended Anode conditions is shown. A DEA can be fed with dry hydrogen, since water crossing through the membrane is sufficient to humidify the fuel. The reduced requirements for inlet humidification yield a system with lower cost and weight compared to FCs with flow-through or recirculated anodes. The accumulation of water and nitrogen in the anode channel is first observed near the outlet. A stratified pattern develops in the channel where a hydrogen-rich area sits above a depleted region and is stabilized by the effect of gravity. A model is presented which describes the dynamic evolution of a blanketing N_2 front in the anode channel and a hydrogen starved region. Understanding, modeling, and predicting the front evolution can reduce the H_2 wasted during purges, avoid over drying the membrane, and mitigate degradation associated with hydrogen starved areas.

Introduction

In this work, the dynamic behavior of low temperature Fuel Cell (FC) operation under Dead-Ended Anode (DEA) conditions are observed and modeled. The fuel utilization of the anode flow-through operation is too low for commercial and portable systems. To increase the fuel utilization, anode recirculation can be employed but the required hydrogen grade plumbing and hardware (ejector/blower) adds weight, volume and expense to the system (1, 2). Additional complexity is also added to the balance of plant with the use of external humidification to prevent over-drying of the membrane. However, a DEA can be fed with dry hydrogen, which is regulated to maintain anode pressure, and the water crossing through the membrane is enough to humidify the fuel. The reduced requirements for inlet humidification yield a system with lower cost and weight.

Nitrogen, from air fed into the cathode, can also cross the membrane, driven by the gradient in partial pressure and accumulate in the channel. Water vapor gradients between the humidified cathode and the dry fed anode also drive excess water into the anode, which can cause significant liquid water accumulation. Unlike water vapor whose maximum partial volume is dictated by temperature, liquid can fill the entire free space and block the flow of reactants, also known as channel plugging. The accumulation of liquid water and nitrogen in the anode channel (AN CH) is observed near the outlet of the channel. As the mass accumulation continues, a stratified pattern, which is stabilized by the effect of gravity, develops in the channel with a hydrogen-rich area sitting above a hydrogen depleted region. A model of the accumulation is presented which

describes the dynamic evolution of water and N_2 blanketing fronts in the anode channel leading to the development of a hydrogen starved region. The prediction of the voltage drop between purge cycles is shown. The model is capable of describing both the two-sloped behavior of the voltage decay and the time at which the steeper slope begins by capturing the effect of H_2 concentration loss and the area of the H_2 starved region along the anode channel.

Purges of the anode channel (AN CH) volume are necessary to clear the reaction product (water) and inert (nitrogen) gas from the channel. An anode purge event consists of opening a downstream solenoid valve, which creates a brief, high velocity flow-through the anode, removing liquid water and nitrogen. After the purge, the catalyst area contributing to the reaction increases and, hence, the measured voltage increases. Understanding, modeling, and predicting the front evolution and overall dynamics in DEA FC would allow judicious choice of purging interval and duration. Better purging strategy can reduce the H_2 wasted during purges and avoid over drying the membrane. The operation of a PEMFC with hydrogen starved areas can also lead to carbon corrosion (3); therefore, the study of these operating conditions and the derivation of controllers to schedule anode purges are critical for DEA operation and prolonging stack life.

Modeling

In this section, a one-dimensional model of nitrogen crossover and accumulation in the AN CH of a DEA PEMFC is presented. The modeling domain for this work is the anode channel, and membrane. Nitrogen crossing though the membrane, into the AN CH, is pushed to the end of the channel by the convective velocity (4). The convective velocity is the result of hydrogen consumption and, therefore, the velocity is greatest near the anode inlet, decreasing along the length of the channel. Due to the high diffusivity of hydrogen in the AN CH, we use the Stefan-Maxwell equation to describe the nitrogen distribution along the channel, resulting from both convection and diffusion, for comparison with the measured mole fractions from GC sampling. A physics based voltage model is used to account for the distributed current density and hydrogen consumption rate. The voltage model includes the effect of membrane water content and proton concentration. We consider an isothermal modeling approach, and the measured cell end plate temperature is used for T.

The important dimensions for channel modeling are x, the through membrane direction, and y, the along-the-channel direction, as shown in Fig. 1. For the anode, the spatial variation of gas concentrations in the x-direction is considered, but the steady-state gas diffusion profiles are calculated and used to propagate the channel values (which are modeled as dynamic states) across the GDL to the surface of the membrane. A similar decoupling between the x and y distributions is proposed in Ref. (5), to address the computational complexity and to take advantage of the very different length scales. On the cathode, only the steady state profiles are considered for modeling both the x- and y-dimensions. The approximation of steady-state distributions is appropriate for the cathode gas channel due to the high gas flow rate and the large time scales over which the anode dynamics evolve.

The constants, listed in Table 2, and equations describing the gas constituents in the channels are written using SI units. The exceptions are the related parameters in the voltage model, Table 1 , which use A cm^{-2} consistent with the FC literature. In the along-the-channel model, the fluxes n have units (mol m^{-1} s^{-1}), and flows N (mol s^{-1}).
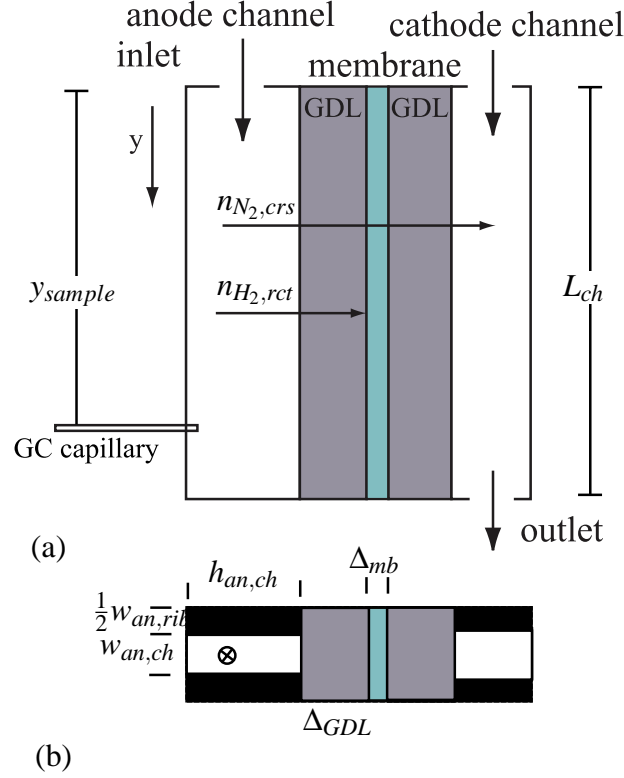
Figure 1: (a) One-dimensional FC modeling domain; y denotes the distance along the channel from inlet to outlet (not drawn to scale). (b) FC channel dimensions.

Nitrogen Accumulation (single phase along the channel model).

To consider both water and nitrogen transport though the membrane, our modeling effort requires consideration of a ternary system for the anode. The Stefan-Maxwell model describes convection, diffusion, and reactions in the gas-channel,

$$\frac{P_{an}}{RT}\frac{\partial x_i}{\partial t} = -\frac{\partial}{\partial y}(J_i + x_i N_t) + r_i, \tag{1}$$

for $i = [1, 2]$, where N_t is the total gas flux, J_i is the diffusive flux, and r_i denotes the reaction terms. Only two of the three components are independent in this modeling framework. We chose the mole fractions of nitrogen, $x_{N_2} = x_1$, and water vapor, $x_{H_2O} = x_2$, as our dynamics states. Because the mole fractions must sum to one,

$$\sum x_i = 1, \tag{2}$$

we can calculate the hydrogen from the other gases $x_{H_2}(y) = 1 - x_{N_2}(y) - x_{H_2O}(y)$. Note that $x_{H_2} = \min(x_2, P_{sat}(T)/P_{an,in})$ is used for all the following calculations, including J_i. The remaining water is assumed to be liquid water and is tracked separately; we are assuming instant condensation.

The convective flux, N_t, is driven by the consumption of hydrogen Eq. 7. In Eq. 1, a constant pressure is used as an approximation because the anode volume is fed via pressure regulation and the straight channel geometry introduces minimal pressure drop along the length of the channel. Although a pressure gradient, corresponding to the convective flux, develops along the length of the channel, the pressure drop is less than 1 Pa at 1 A cm^{-2}, so a constant pressure is valid for

calculating the concentrations. The ideal gas law, $PV = nRT$ or $P = cRT$, is used to relate pressure and mole fraction of gas species in the channel.

A causal formulation for the diffusive fluxes is used (6)

$$\begin{bmatrix} J_1 \\ J_2 \end{bmatrix} = -\frac{P_{an}}{RT\phi(x)} \begin{bmatrix} D_1(x_1), & D_2(x_1) \\ D_3(x_2), & D_4(x_2) \end{bmatrix} \begin{bmatrix} \frac{\partial x_1}{\partial y} \\ \frac{\partial x_2}{\partial y} \end{bmatrix}, \quad [3]$$

where

$$\begin{aligned}
D_1(x_1) &= (1-x_1)D_{13}D_{12} + x_1 D_{23}D_{13}, \\
D_2(x_1) &= -x_1(D_{23}D_{12} - D_{23}D_{13}), \\
D_3(x_2) &= -x_2(D_{13}D_{12} - D_{23}D_{13}), \\
D_4(x_2) &= (1-x_2)D_{23}D_{12} + x_2 D_{23}D_{13},
\end{aligned} \quad [4]$$

and D_{ij} are the temperature-dependent binary diffusion coefficients from Ref. (7). $\phi(x)$ is given by

$$\phi(x) = (D_{23} - D_{12})x_1 + (D_{13} - D_{12})x_2. \quad [5]$$

Conservation of mass allows solving of Eq. 1 for $N_t(y)$, assuming the outlet flow is known $N_t(L) = N_{out}$. The equation for conservation of mass can be written as,

$$\frac{\partial N_t}{\partial y} = \sum r_i, \quad [6]$$

becasue $\sum J_i = 0$ by definition. Then the convective flux along the channel can be found from Eq. 6 by integrating backward in space along the channel,

$$N_t(y) = N_t(L) + \int_y^L \left(n_{H_2,rct}(\tilde{y}) + n_{N_2,crs}(\tilde{y}) + n_{H_2O,crs}(\tilde{y}) \right) d\tilde{y}. \quad [7]$$

Since the anode is dead-ended, $N_{out} = 0$ unless the downstream solenoid valve is open and the anode is purging, in which case $N_{out} = N_{purge}$, a constant.

The source term for nitrogen in the AN CH is membrane crossover, which is calculated from the difference in nitrogen partial pressure across the membrane of thickness Δ_{mb},

$$n_{N_2,crs}(y) = -K_{N_2}(T, \lambda_{mb})(w_{an,ch} + w_{an,rib}) \cdot \frac{(P_{N_2,ca,mb}(y) - P_{N_2,an,mb}(y))}{\Delta_{mb}}. \quad [8]$$

We assume that the permeation takes place both over the ribs and channels $(w_{an,ch} + w_{an,rib})$, where w_* indicates the width of each. The partial pressure of nitrogen at each membrane surface is calculated using the following expressions, $P_{N_2,an,mb}(y) = x_{N_2}(y) P_{an,in}$ and $P_{N_2,ca,mb}(y) = P_{ca,in} - P_v(T) - P_{O_2,ca,mb}(y)$, assuming uniform pressure and saturated water vapor everywhere. This is reasonable, considering the water generation rate, especially when humidified inlets are used at low to mid temperatures. The oxygen concentration at the cathode surface of the membrane, $P_{O_2,ca,mb}(y)$, is calculated using Eq. 26. The nitrogen permeation rate, $K_{N_2}(T, \lambda_{mb})$, is given by Eq. 30, and depends both on temperature and membrane water content.

The hydrogen reaction rate is calculated from the local current density,

$$n_{H_2,rct}(y) = \frac{i_{fc}(y)}{2F}(w_{an,ch} + w_{an,rib}), \quad [9]$$

where F is Faraday's constant.

The source term for water vapor in the AN CH is also membrane crossover, which is calculated from the diffusion and electro-osmotic drag

$$n_{H_2O,crs} = -\left(\frac{\lambda_{ca} - \lambda_{an}}{R_{w,mb}} - n_d(\lambda_{mb})\frac{i_{fc}}{F}\right)(w_{an,ch} + w_{an,rib}) \qquad [10]$$

where $R_{w,mb}$ is the resistance to membrane transport,

$$R_{w,mb} = \frac{\Delta_{mb}}{D_w(\lambda_{mb}, T)} + \frac{1}{k_{ads}} + \frac{1}{k_{des}}, \qquad [11]$$

arising from diffusion, where $D_w(\lambda_{mb}, T)$ is the water diffusion coefficient for water in the membrane (8) and interfacial mass transfer attributed to membrane adsorption k_{ads} and desorption k_{des} (8, 9, 10).

The coefficient of electro-osmotic drag, $n_d(\lambda_{mb})$, can also be found in Ref. (8). Both D_w and n_d are λ_{mb} dependent and increase with membrane water content.

The membrane water content is the final dynamic state in the model and is calculated from the difference between the anode and cathode equilibrium lambda values

$$\frac{\partial \lambda_{mb}(y)}{\partial t} = K_{mb}(\lambda_{an}(y) + \lambda_{ca}(y) - 2\lambda_{mb}(y)) \qquad [12]$$

where $K_{mb} = k_{ads}/\Delta_{mb} = 0.25$ is the membrane water uptake rate. Other, more recent models for membrane water uptake (9, 10), will be investigated in a future work but should not impact the results for nitrogen accumulation presented here.

The equilibrium membrane water content is calculated from the water activity using the uptake isotherm (8)

$$\lambda_{an}(y) = c_0(T) + c_1(T)a_{H_2O,an} + c_2(T)a_{H_2O,an}^2 + c_3(T)a_{H_2O,an}^3 \qquad [13]$$

where $a_{H_2O,an}(y) = x_{H_2O}(y) P_{an,in}/P_{sat}(T)$.

There exists a coupling between membrane water content, $\lambda_{mb}(y)$, the current density distribution, $i_{fc}(y)$, and nitrogen crossover rate, $K_{N_2}(T, \lambda_{mb})$. The nitrogen permeation rate depends on membrane water content, and the nitrogen accumulation rate depends on both the permeation rate and current density distribution (convective vs diffusive flow). The current density distribution depends on nitrogen accumulation (through blanketing of H_2) and the membrane water content for proton transport losses in the membrane. Finally the membrane water content depends on the local current density and channel / GDL conditions.

Modeling the GC sample location

The flow of gas removed from the AN CH during sampling is modeled by modifying Eq. 7 to include the sample flow

$$N_t(y) = N_t(L) + \int_y^L (n_{H_2,rct}(\tilde{y}) + n_{N_2,crs}(\tilde{y}) + n_{H_2O,crs}(\tilde{y}))d\tilde{y} + \begin{cases} N_{sample} & \text{for } (y \leq y_{sample}) \\ 0 & \text{for } (y > y_{sample}) \end{cases} \qquad [14]$$

where y_{sample} is the location of the sampling port along the equivalent channel.

Because the FC is on a 45 ° angle and each of the AN CHs is connected at the top and bottom, as shown in Fig. 2, the N_2 blanketing front propagation needs to be transformed for comparison with an equivalent straight single channel. The nitrogen coverage area, however, can be directly related to the coverage area in the single channel equivalent model. Hence, we use the following relationship for the virtual single channel fuel cell sampling location y_{sample},
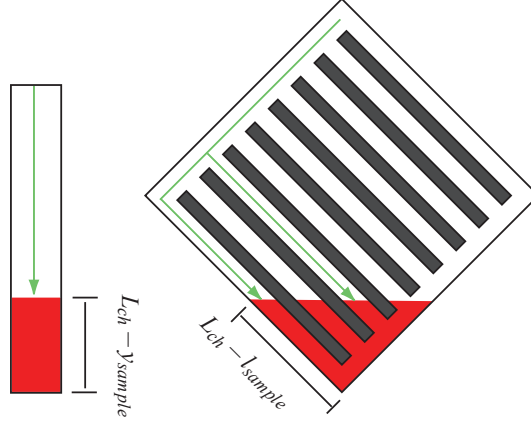

Figure 2: Mapping AN CHs to equivalent single channel. The path length, in the 45° orientation, to nitrogen front location is the same for all channels.

$$\frac{(L_{ch} - y_{sample})}{L_{ch}} = \frac{(L_{ch} - l_{sample})^2}{2A_{fc}} \ . \tag{15}$$

This equation relates the fractional area below the sampling location for the fuel cell placed in the diagonal orientation (right), as shown in Fig. 2, to the fractional area below the sampling location in the equivalent model (left), as shown in Fig. 1. The physical nitrogen sampling location is 3 cm from the bottom edge of the FC along the last channel, $L_{ch} - l_{sample} = 0.03$, as shown in Fig. 2.

Distributed Current Density

In a previous work, the voltage was calculated based on a uniform apparent current density (11), which is related to the catalyst area with sufficient reactants to support the reaction, i.e., the channel length not covered by nitrogen (4) or water (11). In this work, we consider the distributed current density, which is calculated directly from the reactant concentrations. Although the apparent area modeling technique captured the correct voltage output behavior of the system, the full distributed current density approach is chosen for this work to match internal model states and the measurement of nitrogen molar fraction during sampling from the AN CH at the fixed sampling location, l_{sample}. The diffusion of hydrogen and nitrogen in the AN CH affects both the current density distribution and GC measurement.

The inputs to the voltage model are: total current $I_{fc}(A)$, temperature T (K), membrane water content distribution $\lambda_{mb}(y)$, hydrogen partial pressure at the membrane surface $P_{H_2,an,mb}(y) = RTc_{H_2,an,mb}(y)$ (Pa), and oxygen partial pressure at the cathode membrane surface $P_{O_2,ca,mb}(y)$

(Pa), which is calculated in Eq. 26. The cell terminal voltage is calculated from the open-circuit potential minus the concentration, over-potential, and ohmic losses.

$$E_{cell} = E_{rev}(y) - \eta_{mb}(y) - \eta_{GDL}(y) - \eta_{act,ca}(y) - \eta_{act,an}(y). \qquad [16]$$

The calculation of the FC terminal voltage and current density distribution requires the additional computation effort to solve $N+1$ simultaneous non-linear algebraic constraint equations, where N is the number of discretized sections used to solve the partial differential equation (PDE) system. The distributed current density is resolved by solving the set of N equations, shown in Eq. 16, for a uniform potential E_{cell} and one equation for the conservation of current

$$\frac{I_{fc}}{A_{fc}} = \frac{1}{L_{ch}} \int_0^{L_{ch}} i_{fc}(y) \mathrm{d}y. \qquad [17]$$

The reversible voltage is given by

$$E_{rev}(y) = E_0 - \frac{RT}{nF} \log\left(\frac{aH_2O(y)}{aH_2(y) \sqrt{(aO_2(y))}} \right). \qquad [18]$$

where $E_0 = 1.229 - (T - T_0)\cdot 2.304 \times 10^{-4}$ (12). The reactant and product activities are calculated from the concentrations $aH_2(y) = c_{H_2,an,mb}(y)/C_{ref,H_2}$, $aO_2(y) = c_{O_2,ca,mb}(y)/C_{ref,O_2}$ and $aH_2O = 1$ because the liquid water product is assumed. The subscript ref refers to the reference quantity, and subscript ca,mb refers to the cathode membrane surface.

To simplify the calculation of cell voltage, a hyperbolic sine function is used for the calculation of over-potentials, $\eta_{act,ca}$ and $\eta_{act,an}$, from the exchange current density, $i_{o,ca}(y)$ and $i_{o,an}(y)$

$$\eta_{act,ca}(y) = \frac{RT}{\alpha_{c,a}nF} \mathrm{asinh}\left(\frac{k_{units}\, i_{fc}(y) + i_{loss}}{2i_{o,ca}(y)} \right), \qquad [19]$$

where, $k_{units} = 100^{-2} \frac{m^2}{cm^2}$ is for units conversion, $i_{fc}(y)$ is the distributed current density from Eq. 17 and i_{loss} is the lost current density due to hydrogen crossover, a tuned parameter which is listed in Table 1. The hyperbolic sine is equivalent to the Butler-Volmer equation when the forward and reverse reaction coefficients ($\alpha_{c,a} = \alpha_{c,c}$) are equal (13).

Although the cathode reaction depends on the oxygen concentration as well as the activity of protons in the membrane (14), the proton activity term is typically neglected because there are sufficiently many protons under the FC normal operation. Because we expect a low hydrogen concentration in the anode near the end of the channel, we include the proton effect on the exchange current density

$$i_{o,ca}(y) = i_{o,ref,ca} \left(\frac{c_{O_2,ca,mb}(y)}{C_{ref,O_2}} \right)^{\gamma_{O_2}} \left(\frac{c_{H^+_{ca,mb}}(y)}{C_{ref,H^+}} \right)^{\gamma_{H^+}} \cdot \exp\left(\frac{-E_c}{R} \left(\frac{1}{T} - \frac{1}{T_0} \right) \right), \qquad [20]$$

where $i_{o,ref,ca}$ is the reference current density, c is the reactant concentration, γ is the concentration parameter, and E_c in the Arrhenius term is the activation energy for hydrogen oxidation on platinum (15). The cathode concentration parameter for the local proton activity ($\gamma_{H^+} = 0.5$) is

given by Ref. (16). The inclusion of proton concentration is required to capture the effect of nitrogen blanketing in the AN CH, which prevents hydrogen from reaching the catalyst layer to supply protons for the reaction. The cathode exchange current density is proportional to the square-root of the local proton activity at the cathode catalyst layer and the proton activity in the cathode catalyst layer depends on the concentration of protons dissolved in the aqueous phase in the membrane, which is proportional to the square root of the hydrogen pressure at the anode membrane surface, for low P_{H_2}, (17); therefore, we approximate this relationship with a hyperbolic tangent function

$$\left(\frac{c_{H^+_{ca,mb}}}{C_{ref,H^+}}\right)^{\gamma_{H^+}} = K_{H_2}\tanh\left(100\frac{c_{H_2,an,mb}}{C_{ref,H_2}}\right). \qquad [21]$$

The constant K_{H_2} is absorbed into the reference current density $i_{o,ref,ca}$. At the limit, when the hydrogen concentration is zero, the proton activity at the anode drops to zero. Thus, when the anode is subjected to local fuel starvation, the hydrogen partial pressure drops; hence, the proton concentration in the cathode decreases. Furthermore, the membrane electrolyte conductivity also decreases due to lower contribution from the proton conduction in the bulk phase akin to increasing electrolyte resistance due to decreasing ionic concentration (14).The overall reduction of proton activity at the cathode ultimately leads to a drop in the local current density near the dead-ended exit of the anode. For constant load current (galvanostatic) conditions, as the power production near the outlet shuts down, the current density increases near the anode inlet, where the membrane is relatively dry, which may lead to higher losses and increased temperature.

Similarly, for the anode side

$$\eta_{act,an}(y) = \frac{RT}{\alpha_{a,a}nF}\operatorname{asinh}\left(\frac{k_{units}\, i_{fc}(y) + i_{loss}}{2i_{o,an}(y)}\right), \qquad [22]$$

where the anode exchange current density is

$$i_{o,an} = i_{o,ref,an}\left(\frac{c_{H_2,an,mb}}{C_{ref,H_2}}\right)^{\gamma_{H_2}}\exp\left(\frac{-E_c}{R}\left(\frac{1}{T} - \frac{1}{T_0}\right)\right). \qquad [23]$$

The membrane resistance is calculated as follows

$$\eta_{mb}(y) = \frac{k_{units}\, i_{fc}(y)\, \Delta_{mb}}{\sigma_{mb}(\lambda_{mb},T)\tanh\left(100 c_{H_2,an,mb}/C_{ref,H_2}\right)} \qquad [24]$$

Again, the hyperbolic tangent is used to approximate the relationship between conductivity and proton concentration (17), and to reflect the effect of increasing electrolyte resistance due to decreasing ion concentration (14). The membrane conductivity $\sigma_{mb}(\lambda_{mb},T)$ is a function of water content using the standard relationship from Springer et al. (18).

Finally, the GDL and contact resistances are lumped into R_{GDL} for the ohmic loss term

$$\eta_{GDL}(y) = k_{units}\, i_{fc}(y)R_{GDL} \qquad [25]$$

The voltage model was tuned using flow through data from the FC then compared with the experimental voltage degradation rates under dead-ended operating conditions. For model tuning with flow through data, it is assumed that the membrane is fully humidified $\lambda(y) = \lambda(T, a = 1)$, where $\lambda(T, a = 1)$ can be found in Ref. (19), and the effects of GDL and cathode catalyst layer flooding are ignored due to the low current density operation.

Along the channel distributions

The oxygen partial pressure in the cathode channel is not presently considered as one of the dynamic states in the model, it is calculated simultaneously with the current density distribution $i_{fc}(y)$ (A/cm^{-2}) from the cathode inlet pressure and SR using

$$P_{O_2,ca,mb}(y) = P_{O_2,ca,in} - \frac{RT}{4F}\left(\frac{i_{fc}(y)}{h_m} + \frac{i_{fc}(y)\Delta_{GDL}}{D_{O_2,eff}} + \int_0^y \frac{i_{fc}(\tilde{y})}{u_{ca,in}h_{ca,ch}}d\tilde{y}\right)\frac{(w_{ca,ch}+w_{ca,rib})}{(w_{ca,ch})} \quad [26]$$

where $h_{ca,ch}$ is the CA CH height, $w_{ca,ch}$ is the CA CH width, and $w_{ca,rib}$ is the cathode rib width. h_m is the interfacial mass-transfer coefficient, (13) and $u_{ca,in}$ is the cathode inlet gas velocity (assumed constant along the length of the cathode channel for simplicity)

$$u_{ca,in} = \frac{SR_{ca}\, I_{fc}\,(w_{ca,ch}+w_{ca,rib})\,L_{ca,ch}(RT)}{(4F)A_{fc}\,P_{O_2,ca,in}\,(h_{ca,ch}w_{ca,ch})} \quad [27]$$

where the partial pressure of oxygen at the cathode inlet is given by $P_{O_2,ca,in} = OMF_{ca,in}(P_{ca,in} - P_{v,ca,in})$. $P_{ca,in}$ is the cathode inlet pressure, and $P_{v,ca,in}$ is the cathode inlet vapor pressure, amd $OMF_{ca,in} = 0.21$ is the oxygen molar fraction. SR_{ca} is the cathode stoichiometry.

The cathode vapor pressure along the length of the channel is calculated similarly,

$$P_{H_2O,ca}(y) \approx \min\left(P_{sat}(T), P_{H_2O,ca,in} + \frac{RT}{4F}\int_0^y \frac{i_{fc}(\tilde{y})}{u_{ca,in}h_{ca,ch}}d\tilde{y}\frac{(w_{ca,ch}+w_{ca,rib})}{(w_{ca,ch})}\right). \quad [28]$$

This equation actually needs $+\int n_{H_2O,crs}(\tilde{y})\,d\tilde{y}$ to be correct, but then it becomes difficult to solve for the steady-state cathode vapor distribution analytically. At high cathode SR, this should not be a problem, but it may affect the O$_2$ distribution in low SR; however, this still should be a second order effect compared to variations in the anode.

The anode channel hydrogen concentration is propagated to the membrane surface assuming a simple diffusion model,

$$c_{H_2,an,mb}(y) = \frac{x_{H_2}(y)P_{an,ch}}{(RT)} - \frac{i_{fc}(y)}{2F}\frac{\Delta_{GDL}}{D_{H_2,eff}}\frac{(w_{an,ch}+w_{an,rib})}{w_{an,ch}} \quad [29]$$

based on the effective diffusivity $D_{H_2,eff} = D_{eff}D_{H_2,N_2}$ (20).

Nitrogen Crossover Rate

Kocha et al. (21) reported a large range of nitrogen permeability, over 1 order of magnitude. The permeation increases with both membrane water content and temperature. Temperature has a larger effect on permeability, when the membrane is well hydrated. In this case, the permeability can change by a factor of 2-5 over the normal range of operating temperatures 30-60 °C. The nitrogen permeation model includes the effects of membrane water content and temperature (22)

$$K_{N_2}(T,\lambda_{mb}) = \alpha_{N_2}(0.0295 + 1.21f_v - 1.93f_v^2) \times 10^{-14} \times \exp\left[\frac{E_{N_2}}{R}\left(\frac{1}{T_{ref}} - \frac{1}{T}\right)\right], \quad [30]$$

where $E_{N_2} = 24000$ J mol^{-1}, $T_{ref} = 303$, R is the universal gas constant, and f_v is the volume fraction of water in the membrane, given by;

$$f_v = \frac{\lambda_{mb}V_w}{V_{mb} + \lambda_{mb}V_w} \qquad [31]$$

where $V_{mb} = EW/\rho_{mb,dry}$ is the dry membrane volume, equivalent weight divided by density, and V_w is the molar volume of water. λ_{mb} is the membrane water content.

A change in permeability could account for the different nitrogen accumulation rates observed via different voltage drop rates, assuming the voltage degradation is caused by nitrogen accumulation. The current density would tend to shift toward the inlet, where the membrane is dry and has lower proton conductivity; hence, there would be increased resistive losses when N$_2$ accumulates in the end of the channel.

Modeling Results

The PDE Eq. 1 is discretized using a central difference in space into $N = 50$ sections and solved using an ode solver. The AN CH model is solved using MATLAB "ode15s", which supports Differential Algebraic Equations (DAEs), of the form

$$M\dot{z} = f(z). \qquad [32]$$

where $z = [x_{N_2,an}, x_{H_2O,an}, \lambda_{mb}, i_{fc}, E_{cell}]^T$, and $M = \text{diag}(I^N, I^N, I^N, 0^N, 0)$, and I^N is the $N \times N$ identity matrix.

Three simulation plots are shown in Fig. 3, and 5, corresponding to operating conditions 3, and 6, respectively. These portions of data are contained within the large data sets shown in (23). The first set is chosen to match the model assumptions of humidified channel conditions but no channel liquid water plugging. The third condition shows some flooding and hence error in the model prediction of voltage, but the overall dynamic voltage behavior is captured quite well by the model ignoring the offset. The first plot in Fig. 3 corresponding to condition 3 shows the measured and predicted voltage in the top subplot and the GC measurement and simulated mole fraction at the sampling location in the bottom subplot. The model agrees very well with the data at this operating condition because no AN CH liquid water accumulation was observed during this period. Figure 4 shows the time evolution of the hydrogen mole fraction distribution and membrane water content over a purge cycle. Three snapshots of the distributions, corresponding to t=1700 s, t=2000 s, and t=2400 s, from the third cycle in Fig. 3 are shown. The "corner" in the voltage trace at t=2000 s, where the rate of voltage degradation increases, indicates that a sufficient amount of nitrogen has accumulated in the channel to create a stratified front and a hydrogen starved region develops at the outlet. Finally, at t=2400 s, the nitrogen front has evolved to cover nearly 20% of the anode channel. At this time, the effect of nitrogen blanketing is clear as the current density (the dashed-dotted line in the third subplot) is shifted.

Figure 5 shows a good match with the GC measurement for repeated sampling. This data set corresponds to lower operating temperature and fully humidified cathode inlet conditions, which exhibit both anode and cathode channel plugging, hence the discrepancy between the modeled and measured voltage. The voltage matching is not very good because the effects of flooding or plugging are not represented in the voltage model. Cathode flooding and plugging are responsible
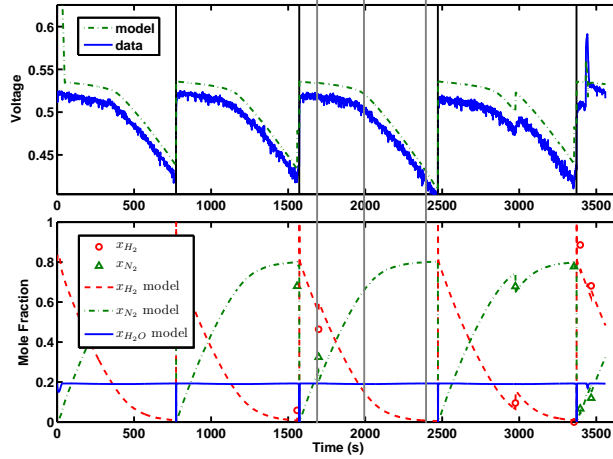
Figure 3: Operating condition 3 (*i*0.6_T65_SR2_RH60) shows very good results with model matching because the assumption of nonwater plugging conditions in the channels is satisfied.
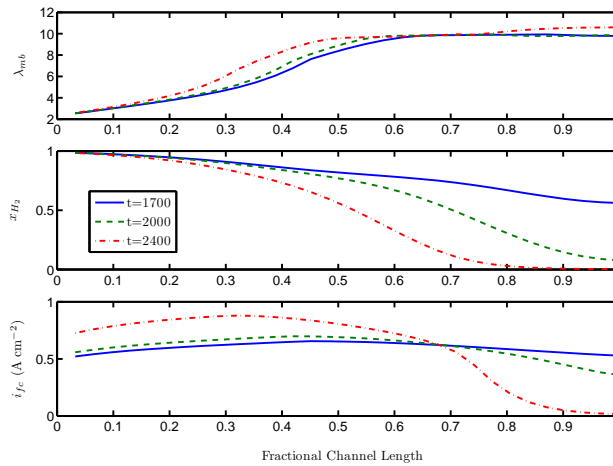

Figure 4: The first subplot shows a snapshot of the membrane water content along the length of the channel for three times, as shown in Fig. 3; after a purge, midcycle, and before the next purge. The second subplot shows the hydrogen mole fraction along the length of the channel. The final subplot shows the current density distributions. The front is fully developed at t=2400 s, leading to hydrogen starved region covering nearly 20% of the channel.

for almost 20 mV of voltage loss, which can be recovered by the cathode surges at t=1000s and t=3400s.

The parameters α_{N_2} and D_{H_2,N_2} affect the rate of nitrogen front propagation and the delay before the voltage decay changes slope, as seen in Fig. 3. Nitrogen front propagation is also weakly dependent on the current density distribution $i_{fc}(y)$, because the consumption of hydrogen drives convection in the channel. The slope of voltage drop depends on membrane/GDL resistance, the nitrogen diffusion rate, and the nitrogen front propagation speed.
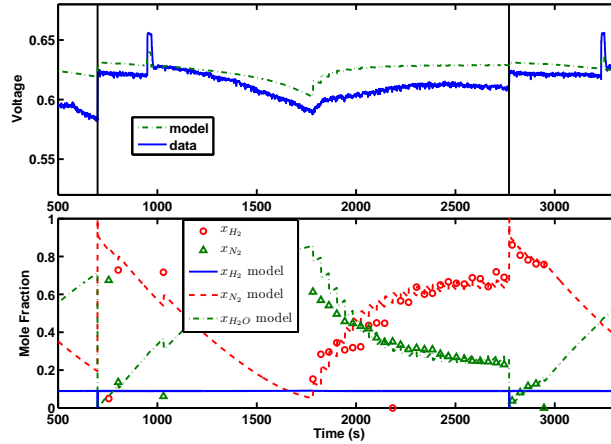
Figure 5: Operating condition 6 (*i*0.4_T50_SR3_RH90): Good agreement with nitrogen measurement during continuous sampling, but poor voltage model matching since flooding effects are not included in the voltage model.

Conclusions

The one-dimensional AN CH model presented in this paper is able to capture and explain the observed two-sloped voltage drop between purges in a PEMFC with DEA. The model shows very good results when the assumption of nonwater plugging conditions are met in the channels. The evolution of a nitrogen blanketing front, which leads to a hydrogen depleted region in the AN CH, explains the voltage loss.

The ability of the model to predict voltage is limited because the accumulation of liquid water in the anode channel (plugging) and cathode catalyst layer (flooding) are not included in the model, but the voltage degradation and nitrogen accumulation rates match well when the assumption of non-flooding and non-plugging conditions are valid. In the future we plan to incorporate these effects into the model. The effects of nitrogen and liquid water accumulation can be parameterized by utilizing the measurement of liquid water from neutron imaging along with the GC measurements for combinations of wet and dry channel conditions. The data set corresponding to operating condition 6, shown Fig. 5, could be used for parameterizing the liquid water effect using the model of nitrogen accumulation, which is calibrated for drier (non-flooding/plugging) conditions.

Appendix: Nomenclature and Constants

Table 1: Tuned Parameters

$i_{o,ref,ca}$	7E-8 (A cm^{-2})	Cathode exchange current
$i_{o,ref,an}$	0.05 (A cm^{-2})	Anode exchange current
i_{loss}	1E-3 (A cm^{-2})	Crossover current
D_{eff}	0.35	Effective Diffusivity in GDL
R_{GDL}	0.275 (Ω cm^2)	Contract resistance
α_{N_2}	2	N$_2$ perm scale factor

Table 2: Constants

E_{N_2}	24000 (J mol^{-1})	(22)
T_{ref}	303 (K)	(22)
R	8.314	Universal gas constant
V_w	1.81×10^{-5}	Water Volume (8)
V_{mb}	5.59×10^{-4}	Membrane Volume (8)
K_{mb}	0.25	Membrane water uptake
n	2	Electron transfer #
F	96485 (C mol^{-1})	Faraday's Constant
C_{ref,O_2}	40.87 (mol m^{-3})	
C_{ref,H_2}	40.87 (mol m^{-3})	
E_c	66000 (J mol^{-1})	(12)
T_0	298.15 (K)	ref Temperature
$\alpha_{a,a}$	0.5	
$\alpha_{c,a}$	0.5	
D_{12}	2.56 E-6 (m^2 s^{-1})	D_{H_2O,N_2} (7)
D_{13}	8.33 E-6 (m^2 s^{-1})	D_{H_2,N_2} (24)
D_{23}	9.15 E-6 (m^2 s^{-1})	D_{H_2O,H_2} (7)
$w_{an,ch}$	0.0021 (m)	An Ch width
$w_{an,rib}$	8.38E-4 (m)	An rib width
Δ_{mb}	25 (μm)	Membrane thickness
$h_{an,ch}$	0.0018 (m)	An Ch height
L_{ch}	0.0727 (m)	Channel length
Δ_{GDL}	3.36E-4 (m)	Compressed GDL thickness
N_{sample}	9.2e-7 (mol s^{-1})	Sample flow rate
N_{purge}	5e-3 (mol s^{-1})	Purge flow rate

References

1. A. Karnik, J. Sun, and J. Buckland, in American Control Conference, American Automatic Council (AACC), p.6 (2006).
2. R. K. Ahluwalia and X. Wang, J. Power Sources, 177, 167 (2008).
3. R. Borup, J. Meyers, B. Pivovar, Y. S. Kim, R. Mukundan, N. Garland, D. Myers, M. Wilson, F. Garzon, D. Wood, et al., Chem. Rev. (Washington, D.C.), 107, 3904 (2007).
4. E. A. Müller, F. Kolb, L. Guzzella, A. G. Stefanopoulou, and D. A. McKay, J. Fuel Cell Sci. Technol., 7, 021013 (2010).
5. P. Chang, G.-S. Kim, K. Promislow, and B. Wetton, J. Comput. Phys., 223, 797 (2007).
6. N. R. Amundson, T.-W. Pan, and V. I. Paulsen, AIChE J., 49, 813 (2003).
7. T. Berning and N. Djilali, J. Electrochem. Soc., 150, A1589 (2003).
8. S. Ge, X. Li, B. Yi, and I.-M. Hsing, J. Electrochem. Soc., 152, A1149 (2005).
9. M. Adachi, T. Navessin, Z. Xie, B. Frisken, and S. Holdcroft, J. Electrochem. Soc., 156, B782 (2009).
10. P. W. Majsztrik, M. B. Satterfield, A. B. Bocarsly, and J. B. Benziger, J. Membr. Sci., 301,93 (2007).
11. D. A. McKay, J. B. Siegel, W. Ott, and A. G. Stefanopoulou, J. Power Sources, 178, 207 (2008).
12. R. P. O'Hayre, S.-W. Cha, W. Colella, and F. B. Prinz, Fuel Cell Fundamentals, John Wiley & Sons, Hoboken, NJ (2006).
13. M. M. Mench, Fuel Cell Engines, John Wiley & Sons, Hoboken, NJ (2008).
14. J. S. Newman, Electrochemical Systems, 2nd ed., Prentice Hall, Englewood Cliffs, NJ (1991).
15. F. Barbir, PEM Fuel Cells: Theory and Practice, Elsevier, Burlington, MA (2005).
16. D. M. Bernardi and M. W. Verbrugge, J. Electrochem. Soc., 139, 2477 (1992).
17. A. Katsaounis, S. Balomenou, D. Tsiplakides, M. Tsampas, and C. Vayenas, Electrochim. Acta, 50, 5132 (2005).
18. T. Springer, T. Zawodzinski, and S. Gottesfeld, J. Electrochem. Soc., 138, 2334 (1991).
19. J. B. Siegel, S. Yesilyurt, and A. G. Stefanopoulou, in Proceedings of Fuel Cell 2009 Seventh International Fuel Cell Science, Engineering and Technology Conference, ASME, p. 439 (2009).
20. J. Nam and M. Kaviany, Int. J. Heat Mass Transfer, 46, 4595 (2003).
21. S. S. Kocha, J. D. Yang, and J. S. Yi, AIChE J., 52, 1916 (2006).
22. R. Ahluwalia and X. Wang, J. Power Sources, 171,63 (2007).
23. J B. Siegel, S. V. Bohac, A. G. Stefanopoulou, and S. Yesilyurt, J. Electrochem. Soc., 157, B1081 (2010).
24. R. Taylor and R. Krishna, Multicomponent Mass Transfer, John Wiley & Sons, New York (1993).